Bulletin of the Seismological Society of America, Vol. 87, No. 5, pp. 1305–1323, October 1997

Hybrid Modeling of *P-SV* Seismic Motion at Inhomogeneous Viscoelastic Topographic Structures

by Peter Moczo, Erik Bystrický, Jozef Kristek, José M. Carcione, and Michel Bouchon

Abstract A new hybrid two-step method for computation of *P-SV* seismic motion at inhomogeneous viscoelastic topographic structure is presented. The method is based on a combination of the discrete-wavenumber (DW), finite-difference (FD), and finite-element (FE) methods. In the first step, the DW method is used to calculate the source radiation and wave propagation in the background 1D medium. In the second step, the FD-FE algorithm is used to compute the wave propagation along the topographic structure.

The accuracy of the method has been separately tested for inclusion of the attenuation and for inclusion of the free-surface topography through numerical comparisons with analytical and independent numerical methods.

The method is a generalization of the hybrid DW-FD method of Zahradník and Moczo (1996) for localized structures with a flat free surface.

Numerical computations for a ridge, sediment valley, and the ridge neighboring the sediment valley show that a ridge can considerably influence the response of the neighboring sediment valley. This means that the neighboring topographic feature should be taken into account even when we are only interested in the valley response.

Introduction

Combination of different computational methods results in hybrid methods that offer advantages not provided by a single method on its own. This is clear from numerous studies presenting a variety of hybrid methods—e.g., Alekseev and Mikhailenko (1980), Ohtsuki and Harumi (1983), Mikhailenko and Korneev (1984), Van den Berg (1984), Kummer *et al.* (1987), Kawase (1988), Gaffet and Bouchon (1989), Emmerich (1989, 1992), Fäh (1992), Fäh *et al.* (1993), Rovelli *et al.* (1994), Bouchon and Coutant (1994), and Zahradník and Moczo (1996).

Zahradník (1995a) and Zahradník and Moczo (1996) developed a hybrid discrete wavenumber–finite-difference method to compute the seismic wave fields at localized 2D near-surface structures embedded in a 1D background medium excited by a point source with arbitrary focal mechanism. The method represents an innovating alternative to the method by Fäh (1992) and Fäh *et al.* (1993). The source radiation and wave propagation in the background medium is calculated by the discrete-wavenumber (DW) method of Bouchon (1981). The wave propagation in and around the localized near-surface structure is calculated by the finite-difference (FD) method. The two-step algorithm is schematically depicted in Figure 1a.

In the article by Zahradník and Moczo (1996), only a flat free surface is considered. In this study, we apply the method to a more general case that includes a free-surface topography and present a hybrid discrete wavenumber–finite-difference–finite-element (DW-FD-FE) method to compute the seismic wave field at localized 2D near-surface anelastic structures with a free-surface topography. Our algorithm is schematically depicted in Figure 1b.

Taking free-surface topography into account can be as important as considering geometry of the sediment-rock interface in the evaluation of site effects for earthquakes and seismic ground-motion modeling. Influence of topography on seismic ground motion has been studied in numerous articles comprehensive list of which can be found in Bouchon *et al.* (1996).

The FD method is widely accepted for modeling seismic wave propagation because, despite its relative simplicity, it is applicable to complex realistic media and, at the same time, it is easy to implement in the computer codes. It is well known, however, that the FD method may have problems with implementing conditions on boundaries of complex geometric shapes. Obviously, the implementation of the boundary conditions is not equally difficult in all specific cases and for all FD schemes.

For example, modeling a staircase free surface in the case of *SH* wave poses no serious problem. An efficient approach for heterogeneous displacement formulations was suggested by Boore (1972)—setting Lamé elastic parameters and density to zero in the grid points above the free

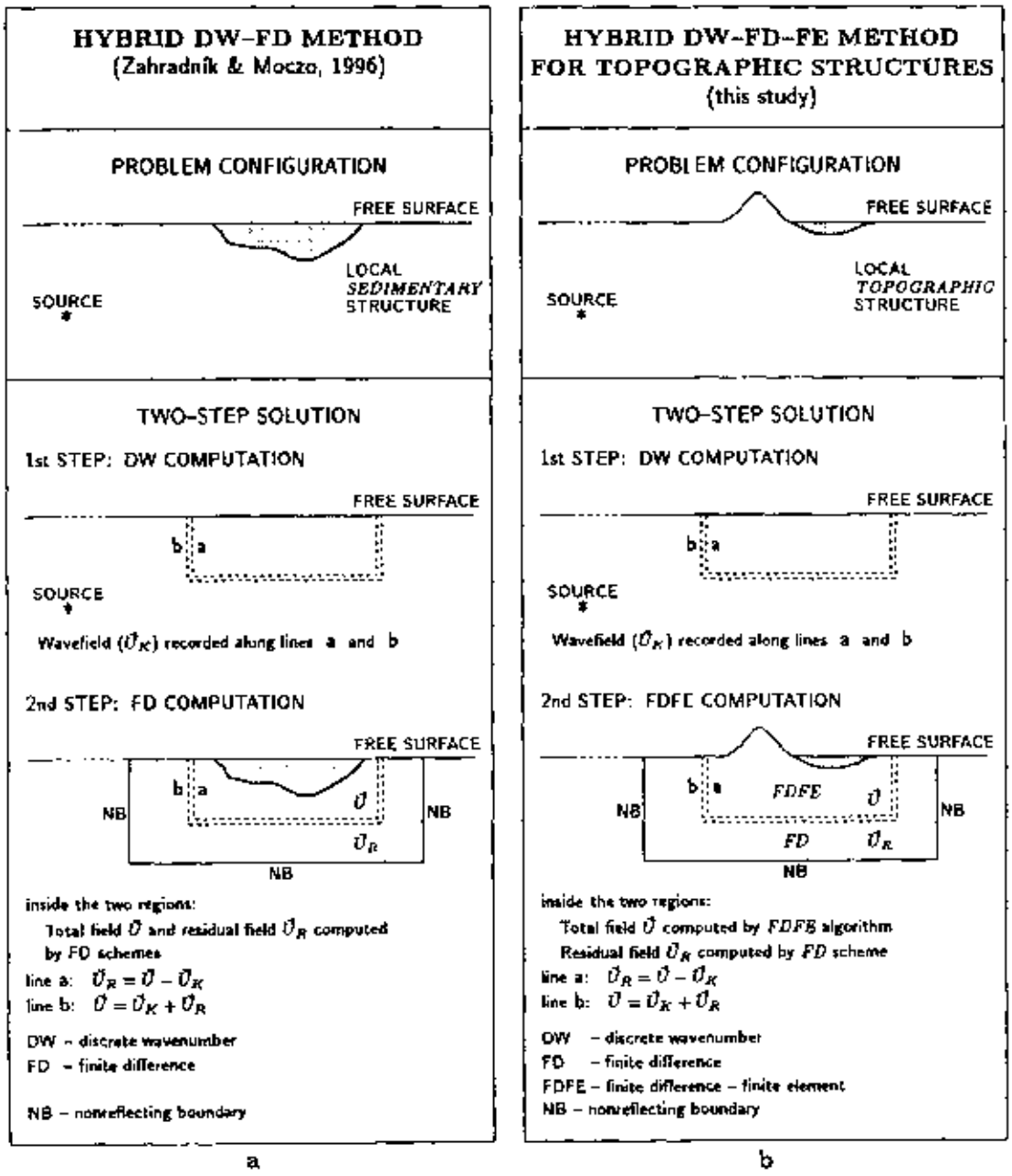

Figure 1. Schemes of the hybrid DW-FD (discrete wavenumber–finite difference) method by Zahradník and Moczo (1996) and the DW-FD-FE (discrete wavenumber–finite difference–finite element) method presented in this study.

surface and using the same scheme for both internal grid points and grid points at the free surface. The approach approximates the traction-free condition reasonably well, and it can be called a vacuum formalism (e.g., Zahradník *et al.*, 1993).

The implementation of the traction-free condition at a nonplanar surface becomes a much more difficult task in the *P-SV* case. This is clear from several studies addressing the problem in the displacement formulation, e.g., Alterman and Rotenberg (1969), Alterman and Loewenthal (1970, 1972), Munasinghe and Farnell (1973), Alterman and Nathaniel (1975), Ilan *et al.* (1975), Ilan and Loewenthal (1976), Ilan (1977, 1978), Fuyuki and Matsumoto (1980), and Jih *et al.* (1988). All articles, except those by Ilan (1977) and Jih *et al.* (1988), treat simple types of the free-surface topography – a quarter and three-quarter planes (i.e., 90° and 270° corners), a (0, 180)-degree wedge, a downward vertical step discontinuity, a valley with a vertical border, and a valley with a steplike border. Nevertheless, the free-surface approximations developed in those studies allowed useful nu-

merical investigations of wave scattering by the FD method, for example, Ilan *et al.* (1979), Ilan and Bond (1981), Boore *et al.* (1981), Fuyuki and Nakano (1984), and Hong and Bond (1986).

Ilan's (1977) treatment of an arbitrary polygonal free surface did not address the transition points between the segments of various slopes and, moreover, required a nonuniform grid that, as noted by Jih *et al.* (1988), decreased accuracy. An improved representation of the arbitrary polygonal free surface was developed by Jih *et al.* (1988). They implemented a traction-free condition using a local rotated coordinate system either parallel to the inclined boundary or aligned with the bisector of the corner. Their approach thus requires a special treatment for each type of line segment and transition point between the sloping segments. Compared to the flat free surface, the accuracy of the approximation is lower and also the range of stable Poisson's ratio is more limited. The technique was used by McLaughlin and Jih (1988) to examine the effect of a near-source topography on short-period seismograms.

An interesting approach to model a free surface of a complicated shape was suggested by John Vidale and used by Frankel and Leith (1992). In order to avoid the tedious explicit implementation of the free-surface condition, they used a density taper above the free surface. Keeping velocities constant and decreasing density to zero when approaching the surface approximates the free-surface condition. The tapering has to be slow enough to prevent instabilities. As Ohminato and Chouet (in press) noted on the tapering technique, putting λ and μ to zero does not always properly simulate a free-surface condition.

Generally, an implementation of free-surface topography in the displacement formulation is not a trivial problem. The more complex geometry, the lower the accuracy and more limitations on the physical parameters of the medium in order to keep the free-surface approximation stable.

The implementation of the traction-free condition is easier and more natural in the velocity-stress FD formulation (Madariaga, 1976; Virieux, 1986; Bayliss *et al.*, 1986). This was pointed out by Bayliss *et al.* (1986) and Levander (1988). Since it is the explicit presence of the stress tensor components in the equations that makes the implementation of the traction-free condition more natural, compared to the displacement formulation, the advantage obviously is not restricted just to the velocity-stress formulation. This is demonstrated by Ohminato and Chouet (in press), who employed the parsimonious staggered grid method of Luo and Schuster (1990) in which the displacement-stress formulation is used instead of the velocity-stress one. Ohminato and Chouet suggested a new way of simply implementing the stress-free condition for a three-dimensional topography. Though much easier than in the displacement formulation, they model topography in a staircase shape.

The noticeable artificial diffraction is generated at the grid-related steps of internal boundaries as was demonstrated by Muir *et al.* (1992). Obviously, steps of the staircase free surface can produce even more pronounced undesired artificial diffraction. This diffraction may not be negligible, especially if the uppermost layer is relatively very soft. The diffraction may consist of a physical diffraction and also, depending on a particular FD scheme, of a numerical diffraction at relatively low frequencies. We observed a nonnegligible diffraction in our FD computations of the *SH* response of the Ashigara Valley and Shidian basin [see Sawada (1992) and Yuan *et al.* (1992), respectively, for the structure characterization]. In our FD computations, the staircase free surface is modeled using the vacuum formalism applied to the heterogeneous, displacement-formulation FD scheme presented in Moczo and Bard (1993). We observe an artificial diffraction at wavelengths up to about 30 times larger than the height of the vertical step of the free surface (equal to the grid spacing). The step-related diffraction may not be obvious in the case of relatively complex wave fields, for example, when the free surface of the ridge is modeled in a staircase shape and no step is isolated from others. We recognized the step-related diffraction on the differential seismograms and also because the steps of the free surface in investigated structures were isolated well enough. An obvious way to lower the diffraction at artificial grid-related steps is to use a relatively small grid spacing, which, of course, may lead to a considerable increase of the total number of the grid points. Using a rectangular grid with varying grid spacings can help to model a staircase free surface that is more conformable to the actual shape, but the efficiency of such a grid, compared to a regular one, is lost as soon as the topographic feature (ridge, hill, or canyon) is covered with a soft surface layer.

The free-surface topography that is not easy to treat in an accurate and stable manner for the FD method is easy and natural for the finite-element (FE) method. When properly employed, the FE method allows using irregular grids with elements of different size, geometry, and even order of approximation. These advantageous features make it possible to treat a traction-free condition on the surface of a complex geometry sufficiently accurately and naturally.

One way to keep advantages of the FD method and, at the same time, to avoid a problematic treatment of the free-surface topography is to combine the FD method with the FE method. This idea is, in fact, not a new one. Ohtsuki and Harumi (1983) and Ohtsuki *et al.* (1984) combined the particle model with the FE method to simulate the *P-SV* wave propagation in a perfectly elastic heterogenous medium with the free-surface topography. In fact, their particle model yields the FD scheme that only differs little from the standard FD scheme for a homogeneous elastic medium in the displacement formulation. Ohtsuki *et al.* (1984) applied the FE method to irregular zones (nonplanar parts of the free surface and internal boundaries) while they used the particle model for the internal homogeneous parts of the medium and homogeneous parts with the horizontal free surface.

In this article, we combine the FE method with the FD method to compute the *P-SV* wave propagation in a visco-

elastic heterogeneous medium with a free-surface topography. We use the FE method to cover fully or partially (e.g., in a narrow strip along the free surface) the topographic feature and the FD method for a major part of the computational region. This means that we use the FD method also for heterogeneous parts of the medium that include material discontinuities.

In the following sections, we first present the equations of motion that govern the *P-SV* wave propagation in the viscoelastic heterogeneous medium. Then we continue with the FD and FE algorithms that solve the above equations of motion. We outline the link between the FD and FE algorithms. In order to test the developed hybrid method, we compare our numerical solutions with those by independent methods. First, we test the incorporation of attenuation in our method using viscoelastic models of an unbounded medium and a half-space. Then, we test the inclusion of free-surface topography using the canyon and ridge models. In the last numerical example, we demonstrate the two-step hybrid computation of the wave field in models including a ridge and a soft valley due to a localized source.

Before we get into the next section, let us note that in this article, we consider only pure 2D problems. Possible extensions to 3D seismic sources are discussed in detail in the article by Zahradník and Moczo (1996). We do not expect any theoretical problem with extending our method to a 3D medium. In a 3D case, however, an efficiency of the computer code becomes a crucial question. The 3D extension of the present method will be addressed elsewhere. Let us point out then that even if we restrict ourselves to a 2D excitation and 2D propagation, it is still advantageous to calculate the source radiation by the DW method because of completeness of the radiated wave field, simplicity and efficiency of the computational scheme, and possibility to simulate complex extended seismic sources.

Equations of Motion

We consider two-dimensional *P-SV* wave propagation in two-dimensionally inhomogeneous viscoelastic medium. Viscoelasticity of the medium allows for the attenuation of waves. Emmerich and Korn (1987) suggested a generalized Maxwell body as a rheological model of the viscoelastic medium suitable to describe realistic attenuation laws in the time-domain computations of wave propagation. In their article, Emmerich and Korn (1987) gave a detailed explanation of the approach as applied to the *SH*-wave propagation. Later, independently, Emmerich (1992) and Fäh (1992) applied the approach to the *P-SV* case. Since we use the time-domain finite-difference and finite-element methods to solve the equations of motion, we adopt the same approach.

Let us note that we applied Emmerich and Korn's method in our previous studies on seismic response of local sedimentary structures—e.g., Zahradník *et al.* (1990), Moczo and Hron (1992), Moczo and Bard (1993), Zahradník *et al.* (1994), Moczo *et al.* (1995), Zahradník and Moczo (1996), and Moczo *et al.* (1996).

Let the computational region be an xz plane and the density ρ and Lamé elastic coefficients λ and μ be dependent on both x and z coordinates. Then the displacement vector $\vec{u}$ ($u[x, z, t]$, 0, $w[x, z, t]$) obeys the equations

$$\begin{aligned} \rho\ddot{u} &= (\kappa u_x)_x + (\mu u_z)_z + (\lambda w_z)_x + (\mu w_x)_z - \sum_{j=1}^{n} \xi_j^u, \\ \rho\ddot{w} &= (\mu w_x)_x + (\kappa w_z)_z + (\mu u_z)_x + (\lambda u_x)_z - \sum_{j=1}^{n} \xi_j^w, \end{aligned} \tag{1}$$

$$\begin{aligned} \dot{\xi}_j^u + \omega_j \xi_j^u &= \omega_j [(\kappa Y_j^\kappa u_x)_x + (\mu Y_j^\mu u_z)_z \\ &\quad + (\lambda Y_j^\lambda w_z)_x + (\mu Y_j^\mu w_x)_z], \\ \dot{\xi}_j^w + \omega_j \xi_j^w &= \omega_j [(\mu Y_j^\mu w_x)_x + (\kappa Y_j^\kappa w_z)_z + (\mu Y_j^\mu u_z)_x \\ &\quad + (\lambda Y_j^\lambda u_x)_z], \quad j = 1, \ldots, n. \end{aligned} \tag{2}$$

Here

$$\kappa = \lambda + 2\mu, \tag{3}$$

and ω_j ($j = 1, \ldots, n$) are the angular relaxation frequencies. The coefficients Y_j^κ and Y_j^μ ($j = 1, \ldots, n$) are obtained, respectively, from the systems of equations

$$\begin{aligned} \sum_{j=1}^{n} \frac{\omega_j \bar{\omega}_k + \omega_j^2 \bar{Q}_\alpha^{-1}(\bar{\omega}_k)}{\bar{\omega}_k^2 + \omega_j^2} Y_j^\kappa &= \bar{Q}_\alpha^{-1}(\bar{\omega}_k), \\ k &= 1, \ldots, 2n - 1, \end{aligned} \tag{4}$$

and

$$\begin{aligned} \sum_{j=1}^{n} \frac{\omega_j \bar{\omega}_k + \omega_j^2 \bar{Q}_\beta^{-1}(\bar{\omega}_k)}{\bar{\omega}_k^2 + \omega_j^2} Y_j^\mu &= \bar{Q}_\beta^{-1}(\bar{\omega}_k), \\ k &= 1, \ldots, 2n - 1. \end{aligned} \tag{5}$$

$\bar{Q}_\alpha(\bar{\omega}_k)$ and $\bar{Q}_\beta(\bar{\omega}_k)$ ($k = 1, \ldots, 2n - 1$) are desired values of the quality factors for P and S waves, respectively, at the specified frequencies $\bar{\omega}_k$. It is reasonable that both the ω_j and $\bar{\omega}_k$ frequencies cover the frequency range of interest logarithmically equidistantly, and $\bar{\omega}_1 = \omega_1$ and $\bar{\omega}_{2n-1} = \omega_n$. The coefficients Y_j^λ ($j = 1, \ldots, n$) are obtained from the relation

$$Y_j^\lambda = \frac{\kappa Y_j^\kappa - 2\mu Y_j^\mu}{\lambda}. \tag{6}$$

The rheology of the medium is represented by two generalized Maxwell bodies. Each of them consists of n classical Maxwell bodies (i.e., n relaxation mechanisms) and a single spring, all connected in parallel. In the generalized Maxwell body, μY_j^μ is the elastic modulus and $\mu Y_j^\mu/\omega_j$ is the viscosity

of the jth classical Maxwell body, and $\mu\left(1 - \sum_{j=1}^{n} Y_j^{\mu}\right)$ is the elastic modulus of the single spring. Analogously, λY_j^{λ}, $\lambda\left(1 - \sum_{j=1}^{n} Y_j^{\lambda}\right)$, and $\lambda Y_j^{\lambda}/\omega_j$ are the elastic moduli and viscosities, respectively, in the other generalized Maxwell body. The viscoelastic modulus of the generalized Maxwell body is

$$M_n(\omega) = M_U\left(1 - \sum_{j=1}^{n} Y_j^{M_U} \frac{\omega_j}{i\omega + \omega_j}\right). \tag{7}$$

$M_n(\omega)$ and M_U stand for $\mu_n(\omega)$ and μ, respectively, in one generalized Maxwell body and for $\lambda_n(\omega)$ and λ in the other. The subscript U means unrelaxed. Then, in one generalized Maxwell body, for example, μ represents the unrelaxed modulus, while the elastic modulus of the single spring, that is, $\mu\left(1 - \sum_{j=1}^{n} Y_j^{\mu}\right)$, represents the relaxed modulus M_R.

In practice, we usually know phase velocities of P and/or S waves at certain reference frequency ω_r (not necessarily the same for both types of waves). Thus, we need a relation between the phase velocities and the corresponding unrelaxed moduli that specify the computational model of the medium. The phase velocity $c(\omega)$ is given by the relation

$$\frac{1}{c(\omega)} = \mathrm{Re}\left[\left(\frac{M_n(\omega)}{\rho}\right)^{1/2}\right]. \tag{8}$$

Then we get from equations (7) and (8)

$$M_U = \rho c^2(\omega_r)\frac{R + \Theta_1}{2R^2}. \tag{9}$$

Here, $R = (\Theta_1^2 + \Theta_2^2)^{1/2}$ and

$$\begin{aligned}\Theta_1 &= 1 - \sum_{j=1}^{n} Y_j^{M_U} \frac{1}{1 + (\omega_r/\omega_j)^2},\\ \Theta_2 &= \sum_{j=1}^{n} Y_j^{M_U} \frac{\omega_r/\omega_j}{1 + (\omega_r/\omega_j)^2}.\end{aligned} \tag{10}$$

If we know the phase velocity for S waves, $c_S(\omega_r)$, then we insert Y_j^{μ} $(j = 1, \ldots, n)$ into equations (10) and get μ from equation (9). If we know the phase velocity for P-waves, $c_P(\omega_r)$, then we insert $Y_j^{\kappa}(j = 1, \ldots, n)$ into equations (10) and get κ from equation (9); λ is then obtained from equation (3).

Numerical Solution

A major part of the computational region is covered by a rectangular grid on which the FD method is used. Topographic irregularities of the free surface are fully or partially covered by, generally, an irregular mesh of finite elements. Both parts of the computational region may include material inhomogeneity.

Finite-Difference Algorithm

Equations (1) and (2) can be solved using the explicit heterogeneous FD scheme suggested recently for perfectly elastic media by Zahradník (1995b) and tested by Zahradník and Priolo (1995). Let u_{il}^m and w_{il}^m be discrete approximations of the displacement components $u(x_i, z_l, t_m)$ and $w(x_i, z_l, t_m)$, $\xi_{j,il}^{u,m}$ and $\xi_{j,il}^{w,m}$ discrete approximations of the functions $\xi_j^u(x_i, z_l, t_m)$ and $\xi_j^w(x_i, z_l, t_m)$, ρ_{il} an effective density at a grid point il, Δt a time step, and Δx, Δz spatial grid spacings. Then we replace differential equations (1) and (2) by their FD approximations:

$$\begin{aligned}u_{il}^{m+1} &= 2u_{il}^m - u_{il}^{m-1}\\ &\quad + \frac{\Delta^2 t}{\rho_{il}}\left[L_{xx}(\kappa,u) + L_{xz}(\mu,u) + L_{zx}(\lambda,w) + L_{zz}(\mu,w)\right.\\ &\quad \left. - \frac{1}{2}\sum_{j=1}^{n}\left(\xi_{j,il}^{u,m+1/2} + \xi_{j,il}^{u,m-1/2}\right)\right];\end{aligned} \tag{11}$$

$$\begin{aligned}w_{il}^{m+1} &= 2w_{il}^m - w_{il}^{m-1}\\ &\quad + \frac{\Delta^2 t}{\rho_{il}}\left[L_{xx}(\mu,w) + L_{zz}(\kappa,w) + L_{xz}(\mu,u) + L_{zx}(\lambda,u)\right.\\ &\quad \left. - \frac{1}{2}\sum_{j=1}^{n}\left(\xi_{j,il}^{w,m+1/2} + \xi_{j,il}^{w,m-1/2}\right)\right];\end{aligned} \tag{12}$$

$$\begin{aligned}\xi_{j,il}^{u,m-1/2} &= \frac{2 - \omega_j\Delta t}{2 + \omega_j\Delta t}\xi_{j,il}^{u,m-3/2} + \frac{2\omega_j\Delta t}{2 + \omega_j\Delta t}\times\\ &\quad \left[L_{xx}(\kappa Y_j^{\kappa},u) + L_{xz}(\mu Y_j^{\mu},u) + L_{zx}(\lambda Y_j^{\lambda},w)\right.\\ &\quad \left. + L_{zz}(\mu Y_j^{\mu},w)\right], \quad j = 1, \ldots, n;\end{aligned} \tag{13}$$

$$\begin{aligned}\xi_{j,il}^{w,m-1/2} &= \frac{2 - \omega_j\Delta t}{2 + \omega_j\Delta t}\xi_{j,il}^{w,m-3/2} + \frac{2\omega_j\Delta t}{2 + \omega_j\Delta t}\times\\ &\quad \left[L_{xx}(\mu Y_j^{\mu},w) + L_{zz}(\kappa Y_j^{\kappa},w) + L_{xz}(\mu Y_j^{\mu},u)\right.\\ &\quad \left. + L_{zx}(\lambda Y_j^{\lambda},u)\right], \quad j = 1, \ldots, n.\end{aligned} \tag{14}$$

If a grid point il is an internal point, the L_{xx}, L_{zz}, L_{xz}, and L_{zx} operators have the form

$$\begin{aligned}L_{xx}(a,f) &= \frac{1}{\Delta^2 x}\left[a_{il}^H(f_{i+1l}^m - f_{il}^m)\right.\\ &\quad \left. - a_{i-1l}^H(f_{il}^m - f_{i-1l}^m)\right],\end{aligned} \tag{15}$$

$$\begin{aligned}L_{zz}(a,f) &= \frac{1}{\Delta^2 z}\left[a_{il}^V(f_{il+1}^m - f_{il}^m)\right.\\ &\quad \left. - a_{il-1}^V(f_{il}^m - f_{il-1}^m)\right],\end{aligned} \tag{16}$$

$$L_{xx}(a,f) = \frac{1}{4\Delta x\Delta z}[a^H_{il}(f^m_{il+1} + f^m_{i+1\,l+1} - f^m_{il-1} - f^m_{i+1\,l-1}) - a^H_{i-1\,l}(f^m_{i-1\,l+1} + f^m_{il-1} - f^m_{i-1\,l-1} - f^m_{il-1})], \quad (17)$$

$$L_{zz}(a,f) = \frac{1}{4\Delta x\Delta z}[a^V_{il}(f^m_{i+1\,l} + f^m_{i+1\,l-1} - f^m_{i-1\,l} - f^m_{i+1\,l}) - a^V_{il-1}(f^m_{i+1\,l-1} + f^m_{il+1} - f^m_{i-1\,l-1} - f^m_{il})], \quad (18)$$

where a^H_{il} and a^V_{il} are the horizontal and vertical effective parameters

$$a^H_{il} = \Delta x\left(\int_{x_i}^{x_{i+1}} \frac{dx}{a(x,z_l)}\right)^{-1}, a^V_{il} = \Delta z\left(\int_{z_l}^{z_{l+1}} \frac{dz}{a(x_i,z)}\right)^{-1}. \quad (19)$$

If the grid point il is at the *flat* free surface, the L_{xx} operator has the same form as in equation (15), but only half-values of the parameters a^H_{il} and $a^H_{i-1\,l}$ in the medium without the free surface have to be considered. The other operators have the form

$$L_{zz}(a,f) = \frac{1}{\Delta z^2}a^V_{il}(f^m_{il+1} - f^m_{il}), \quad (20)$$

$$L_{xz}(a,f) = \frac{1}{4\Delta x\Delta z}[a^H_{i-1/2\,l}(f^m_{il+1} + f^m_{i+1\,l+1} - f^m_{il} - f^m_{i+1\,l}) - a^H_{i-1/2\,l+1}(f^m_{il+1} + f^m_{i-1\,l+1} - f^m_{il} - f^m_{i-1\,l})], \quad (21)$$

$$L_{zx}(a,f) = \frac{1}{4\Delta x\Delta z}[a^V_{i-1/2\,l}(f^m_{il} + f^m_{i+1\,l} - f^m_{i+1\,l} - f^m_{i-1\,l+1}) + a^V_{i-1/2\,l}(f^m_{i+1\,l} + f^m_{i-1\,l+1} - f^m_{il} - f^m_{il+1})], \quad (22)$$

The operators for the flat free surface follow from the application of the vacuum formalism to the full-form FD scheme of Zahradník (1995b).

Since the above schemes for the displacement components are second-order accurate both in space and time, the number of grid points per minimum wavelength and time step are controlled by the standard dispersion and stability relations. In all numerical computations, we used

$$\Delta s \leq \frac{\beta_{\min}}{12f_{\max}} \quad \text{and} \quad \Delta t \leq \frac{0.9\Delta s_{\min}}{(\alpha^2_{\max} + \beta^2_{\max})^{1/2}}, \quad (23)$$

where Δs stands for Δx and Δz, β and α are, respectively, the S-wave and P-wave velocities in a medium, and $f_{\max}$ is the frequency up to which we want to have our computation sufficiently accurate.

If the FD scheme is used in combination with the FE algorithm described below, a more restrictive condition for Δt has to be used.

Finite-Element Algorithm

In the FE method (e.g., Zienkiewicz and Taylor, 1989; Smith, 1975; Serón *et al.*, 1989, 1990, Serón and Badal, 1992), in the case of a perfectly elastic medium, we solve the system of the second-order, linear, ordinary differential equations

$$\mathbf{M}\ddot{\mathbf{d}} + \mathbf{K}\mathbf{d} = \hat{\mathbf{f}} \quad (24)$$

instead of the second-order, linear partial differential equation of motion

$$\rho\ddot{u}_i = \sigma_{ij,j} + f_i. \quad (25)$$

In equation (24), $\mathbf{M}$ is the mass matrix determined by the density distribution in the medium, $\mathbf{K}$ is the stiffness matrix determined by the elastic properties of the medium, $\mathbf{d}$ is the displacement vector consisting of discretized displacements in the nodes, and $\hat{\mathbf{f}}$ is the load vector determined from the source and boundary conditions. Therefore, the vector $\hat{\mathbf{f}}$ is present in the system of equations (24) even if the body force term f_i is not considered in equation (25) (as in the case of equations 1). $\sigma_{ij,j}$ stands for the partial spatial derivatives of the stress tensor.

It is obvious that in a general case, a solution of equation (24) may be inconsistent with a solution of equation (25): the solution of equation (24) may not be as smooth as the solution of equation (25) if certain conditions for the right-

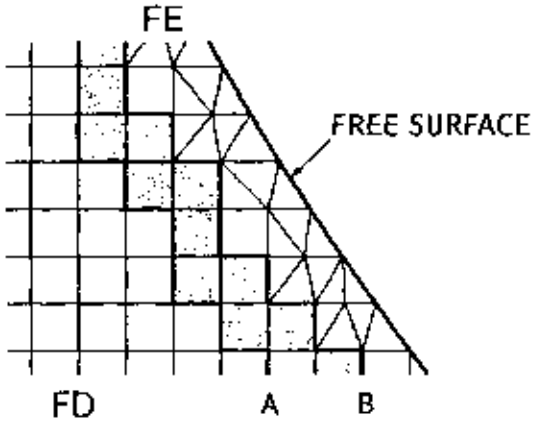

Figure 2. Contact between the regions covered by the finite-difference and finite-element grids.

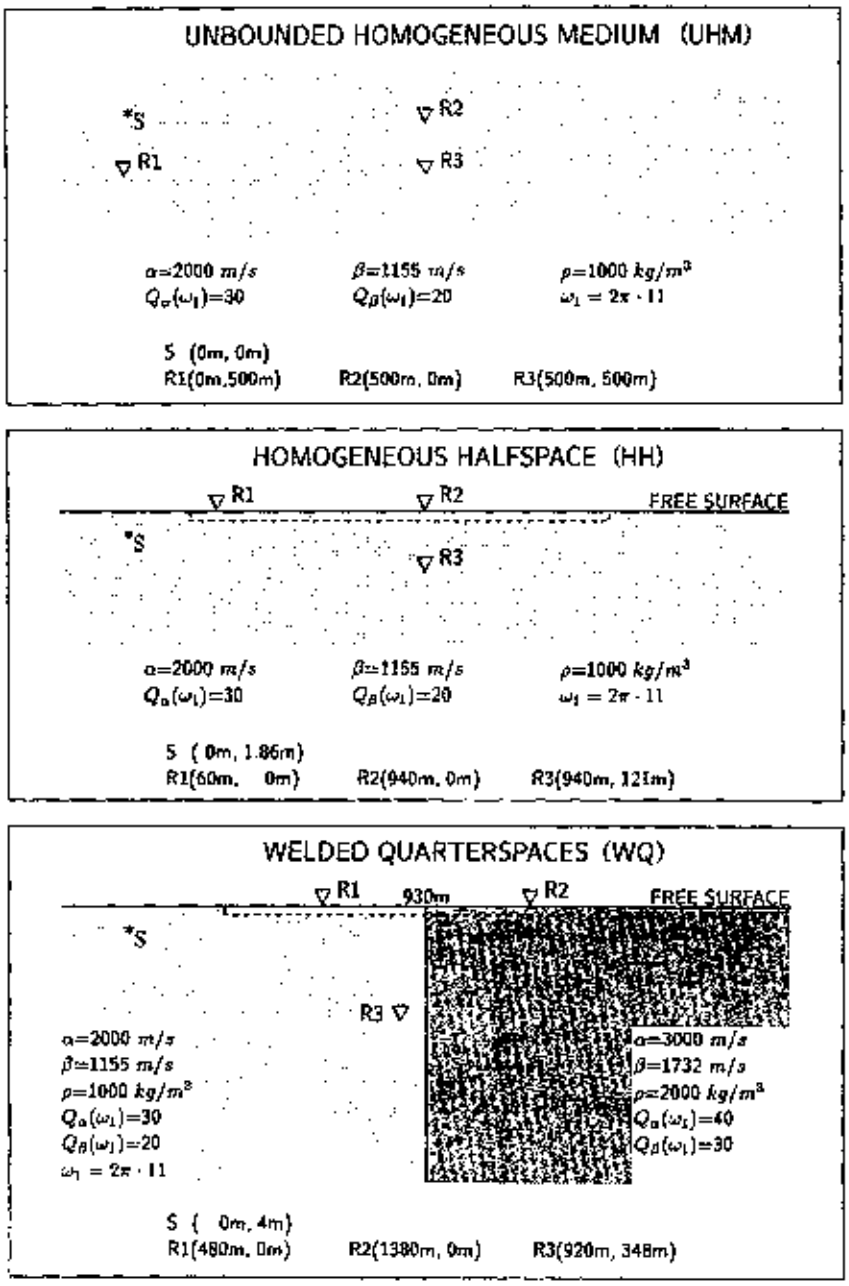

Figure 3. Three models used to test the inclusion of the attenuation. The dashed lines indicate the area covered by the finite elements in the FD FE modeling.

hand side of equation (24) and a border of the solution domain are not satisfied. Consistency of both solutions is principally guaranteed if the border of the solution domain is sufficiently smooth and if the domain itself can be sufficiently well approximated by a convex polygon. As it follows from the numerical experiments, however, good results can be obtained even in the case when the above condition is not satisfied—see, for example, the case of the trapezoidal ridge in the section on test computations.

Since we want to combine the FE method with the FD method, we have to use the same attenuation in both—the FE and FD—computational regions. Referring to equations (1), we add the additional term to the load vector $\hat{\mathbf{f}}$ in equation (24)

$$\mathbf{M}\ddot{\mathbf{d}} + \mathbf{K}\mathbf{d} = \hat{\mathbf{f}} - \sum_{j=1}^{n} \dot{\hat{\xi}}_j, \tag{26}$$

where $\hat{\xi}_j$ is the vector consisting of discretized functions ξ_j in the nodes. It satisfies equations (compare with equations 2)

$$\dot{\hat{\xi}}_j + \omega_j \hat{\xi}_j = -\omega_j \mathbf{K}_j^{\gamma} \mathbf{d}, \quad j = 1, \ldots, n, \tag{27}$$

where $\mathbf{K}_j^{\gamma}$ is the modified stiffness matrix. The $\mathbf{K}_j^{\gamma}$ matrix is defined in the same way as the stiffness matrix except that the elasticity matrix (relating the stress and strain in the ma-

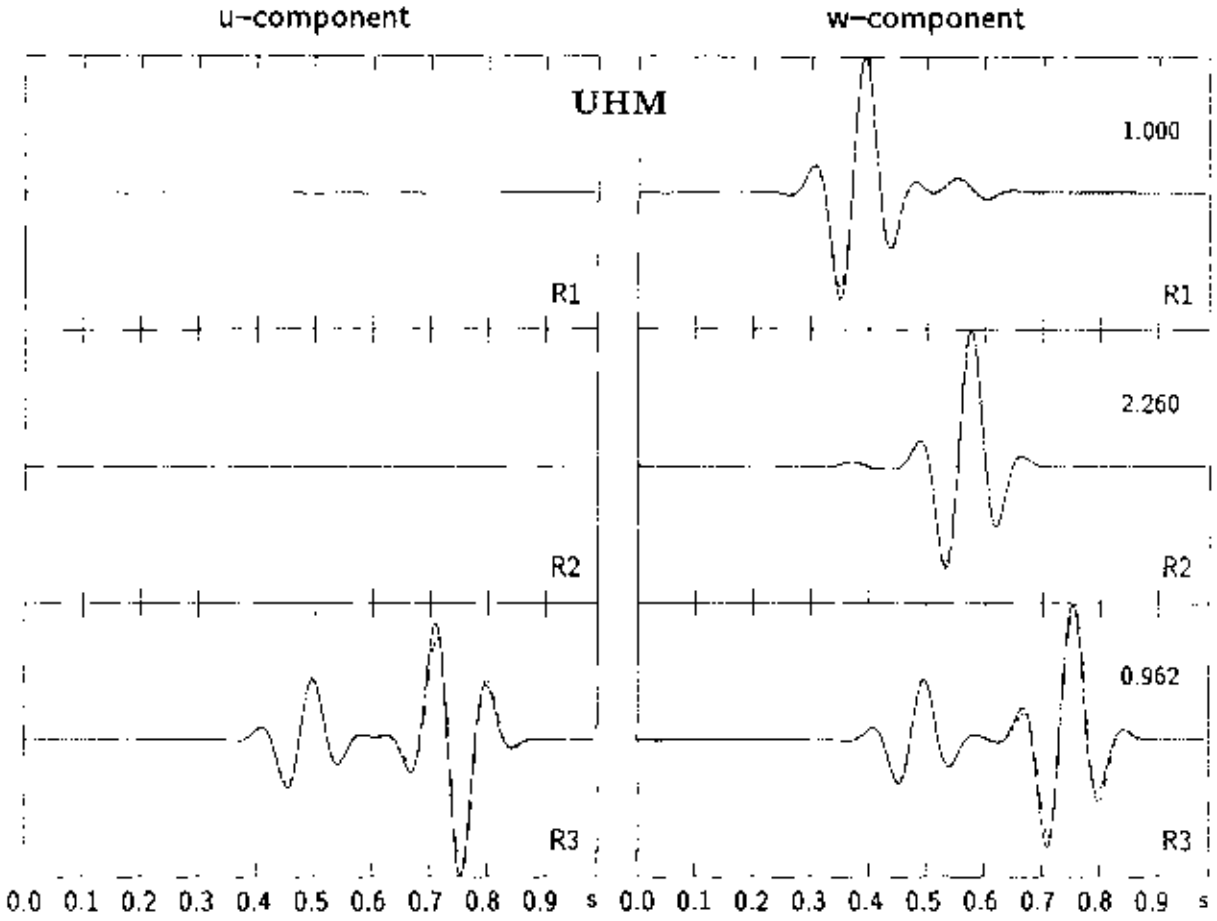

Figure 4. Comparison of three solutions for the models shown in Figure 3. (a) u and w components of the displacements in the three receivers R1 to R3 in the model of an unbounded homogeneous medium (UHM). FD solution, solid line; analytical solution, dashed line. (b) u and w components of the displacements in the three receivers R1 to R3 in the models of the homogeneous half-space (HH) and welded quarter-spaces (WQ). FD solution, solid line; FD-FE solution, long-dash line; the pseudospectral technique (Carcione, 1992), short-dash line. In all cases, the u and w components are scaled separately of each other.

trix formulation of Hooke's law) is replaced by the modified elasticity matrix

$$\begin{pmatrix} Y_j^n\kappa & Y_j^n\lambda & 0 \\ Y_j^n\lambda & Y_j^n\kappa & 0 \\ 0 & 0 & Y_j^n\mu \end{pmatrix}.$$

Several different time integration schemes can be used to integrate equation (26), see Serón *et al.* (1989, 1990). We use the central difference scheme because we need to link the calculations by the FE method with that by the FD method at the contact of the two corresponding computational regions during the process of time integration. In the central difference scheme, as applied to equation (26), we solve a sparse symmetric system of linear equations

$$\frac{1}{\Delta^2 t}\mathbf{M}\mathbf{d}^{m+1} = \mathbf{b}, \tag{28}$$

where

$$\mathbf{b} = \hat{\mathbf{f}}^m - \left(\mathbf{K} - \frac{2}{\Delta^2 t}\mathbf{M}\right)\mathbf{d}^m - \frac{1}{\Delta^2 t}\mathbf{M}\mathbf{d}^{m-1} - \frac{1}{2}\sum_{j=1}^{n}\left(\hat{\xi}_j^{m+1/2} + \hat{\xi}_j^{m-1/2}\right). \tag{29}$$

The time step Δt has to satisfy the stability condition (Bamberger *et al.*, 1980)

$$\Delta t \leq \frac{\Delta x_{\min}}{[3(\alpha_{\max}^2 + \beta_{\max}^2)]^{1/2}}. \tag{30}$$

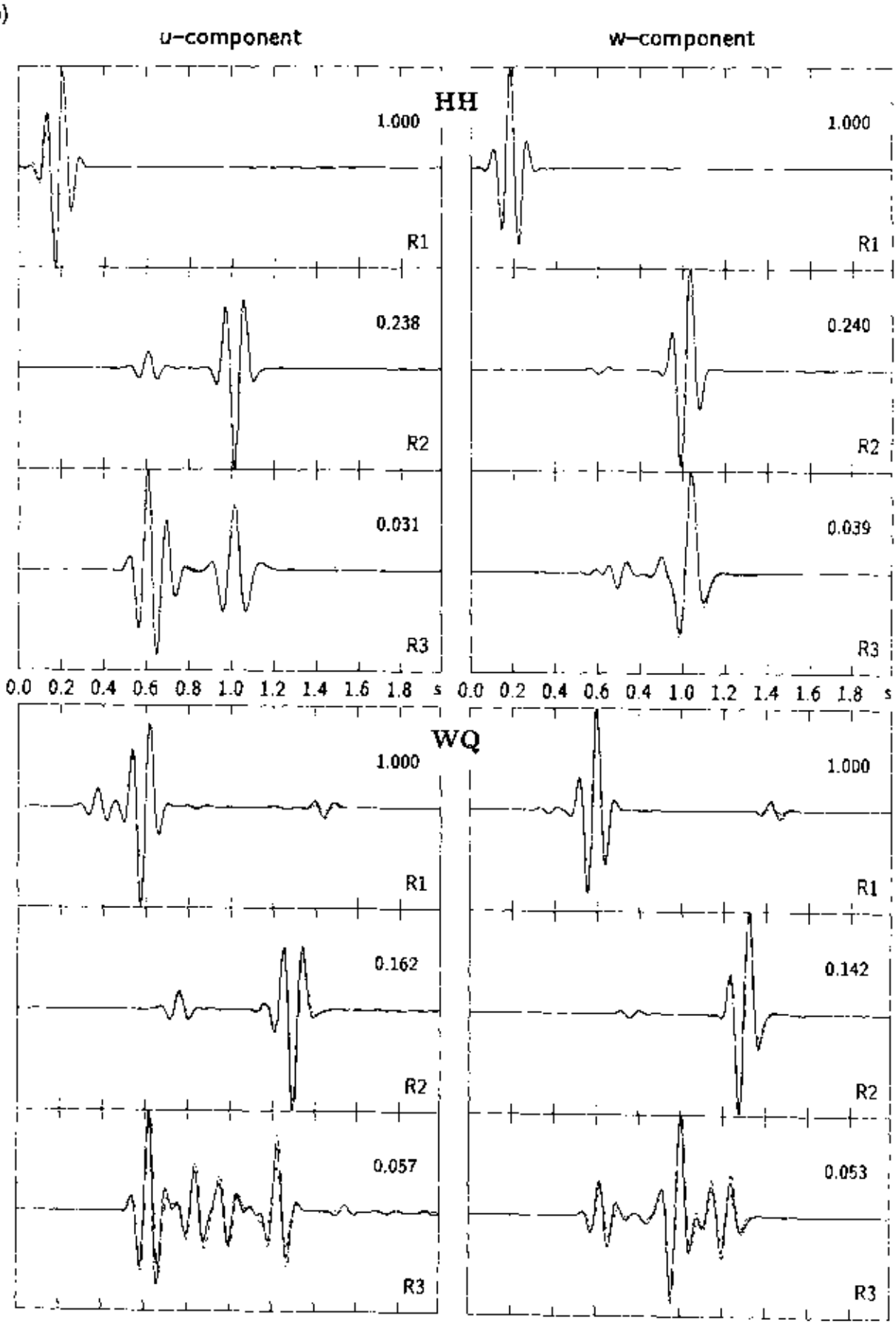

Figure 4. Continued.

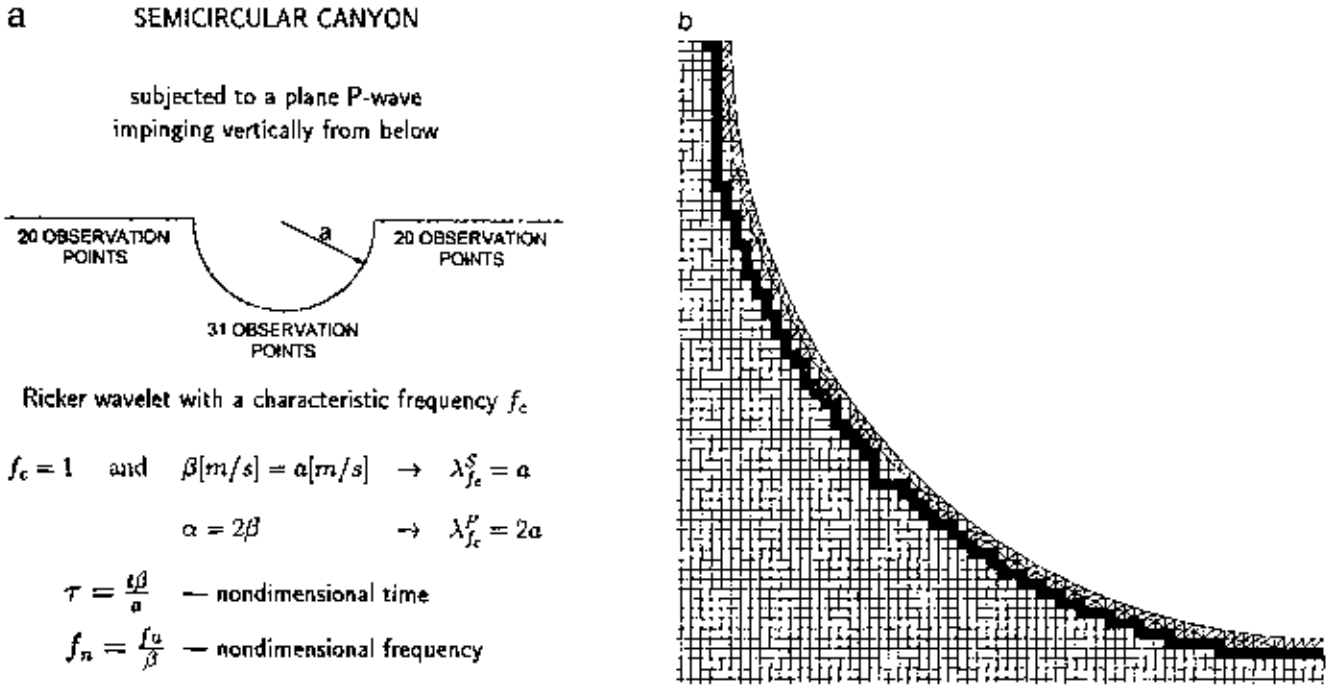

Figure 5. Model of a semi-circular canyon. (a) Geometry and receiver positions. (b) Part of the spatial grid. The shaded area is a transition zone between the finite elements and finite-difference grid as in Figure 2.

As mentioned earlier, this condition is more restrictive than the one (equation 23) for the FD scheme. As in the FD grid, we use 12 elements per minimum wavelength.

We approximate the time derivative of $\hat{\dot{\xi}}_j$ and the function $\hat{\xi}_j$ itself in equations (27) in the same way as $\dot{\xi}_j$ and ξ_j in equations (2). This leads to equations

$$\hat{\xi}_j^{m+1/2} = \frac{2 - \omega_j \Delta t}{2 + \omega_j \Delta t} \hat{\xi}_j^{m-1/2} - \frac{2\omega_j \Delta t}{2 + \omega_j \Delta t} \mathbf{K}_j^T \mathbf{d}^m, \quad j = 1, \ldots, n.$$

Link between the Finite-Difference and Finite-Element Algorithms

The FD and FE algorithms have to communicate at the contact of the two corresponding computational regions during the entire process of time integration. We describe the link using the example of a portion of the computational grid around the free surface of the semicircular canyon shown in Figure 5. The portion of the grid is shown in Figure 2. Nodes on line A are internal for the FD algorithm. At the same time, they are Dirichlet-boundary nodes for the FE region. Therefore, the FE algorithm requires the displacement values calculated by the FD algorithm at these nodes as well as the acceleration values. The accelerations have to be calculated from the displacements with the second-order accuracy. Therefore, we approximate the acceleration in a node at the mth time level for which we use a central difference formula and displacements at the time levels $m - 1$, m, and $m + 1$ in the same node. This implies the use of the above-mentioned central difference scheme for the time integration. The time integration procedure can be then summarized in the following steps:

1. calculation of displacements at time level $m + 1$ from those at time levels $m - 1$ and m in the FD region;
2. calculation of accelerations at the mth time level in the nodes on line A;
3. calculation of displacements in the FE region at time level $m + 1$ from the displacements at time levels $m - 1$ and m and from boundary conditions at the mth time level; and
4. prescribing displacements at time level $m + 1$ in the nodes on line B as a boundary condition for the FD region.

It is obvious that covering certain parts of the computational region by finite elements instead of a finite-difference grid implies some additional costs— increase in computational time and memory requirements. Let us consider M points in the FD grid. Consider then that we replace N grid points by N nodes of finite elements. Restrict ourselves to perfectly elastic medium since, in principle, the attenuation may be introduced in different ways—not necessarily using the rheology of the generalized Maxwell body. In our FD scheme, each grid point is assigned seven values (effective density, three horizontal and three vertical harmonic averages of elas-

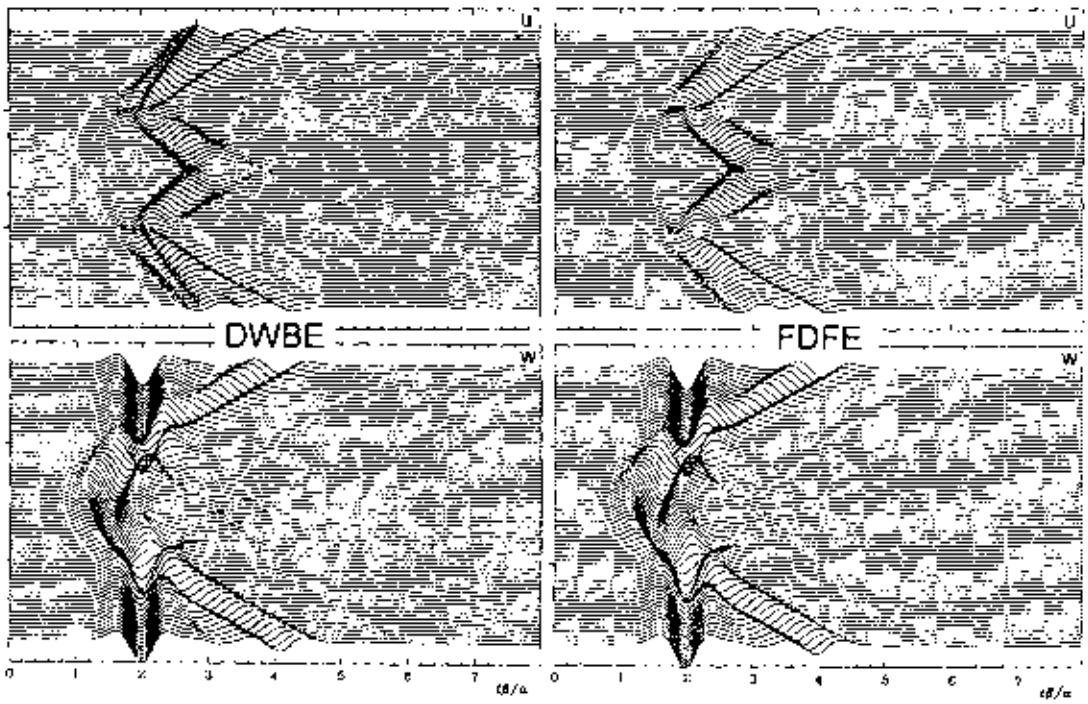

Figure 6. Comparison of the DW-BE (discrete wavenumber boundary element) solution by Kawase (1988, Fig. 12) and our FD-FE solution for the model of the semicircular canyon shown in Figure 5.

tic moduli) describing medium properties. For N finite-element nodes, we construct mass and stiffness matrices. Then the lumped mass matrix consists of $2N$ nonzero values. The maximum number of nonzero values in the stiffness matrix— $2N \times 18$—gives the upper estimate of number of values that have to be stored in core memory. Depending on the medium and finite-element mesh, the number of nonzero values in the stiffness matrix may be lower usually by 10%. Thus, an increase in memory requirement is controlled by the number of finite-element nodes and the finite-element mesh (shapes of elements and their configuration). Based on our computational experience, we can approximately estimate the ratio of memory requirements in the combined FD-FE grid to those in an equivalent FD grid as

$$\frac{M + 4N}{M}.$$

Similarly, we estimate the ratio of the computational times as

$$\frac{M + 6N}{M} \frac{\Delta t_{FD}}{\Delta t_{FE}},$$

where Δt_{FD} and Δt_{FE} are time steps according to equations (23) and (30). We conclude that it is desirable to use finite elements only for a small portion of the entire computational region.

Test Computations

In order to test the accuracy of the developed method, we compare numerical results for selected problems with results obtained by independent methods of calculation.

Inclusion of Attenuation

First we consider a model of an unbounded homogeneous medium and two half-space models— a homogeneous and a welded quarter-space models. The elastic parameters and wave-field excitation in the half-space models are taken from the article by Zahradnik and Priolo (1995). All the models are shown in Figure 3. In all cases, the wave field is excited by a line source. The source is a vertical body force. Its time dependence in the case of the unbounded medium is given by a zero-phase Ricker wavelet

$$f_w(t) = \exp[-0.5f_0^2(t - t_0)^2] \cos[\pi f_0(t - t_0)],$$

where $f_0 = 22$ Hz and $t_0 = 0.136$ sec. In both half-space models, the source is applied near the surface. Its time function is given by the first derivative of the above Ricker wavelet

$$f_w(t) = \cdot \exp(b)f_0[f_0 \cos(c)(t - t_0) + \pi \sin(c)],$$

$$b = -0.5f_0^2(t - t_0)^2, \quad c = \pi f_0(t - t_0),$$

with $f_0 = 22$ Hz and $t_0 = 0.136$ sec.

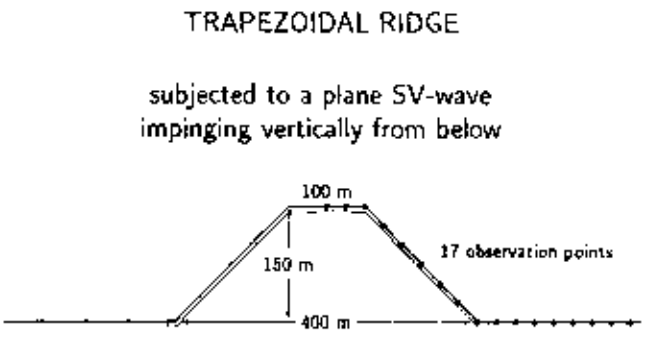

Figure 7. Model of a trapezoidal ridge- –geometry and receiver positions. The shaded area indicates the strip covered with the finite elements.

For an unbounded medium, we compare the FD solution with the corresponding analytical solution (e.g., Carcione *et al.*, 1988). The comparison is shown in Figure 4a. Both solutions are in very good agreement.

In the case of the viscoelastic Lamb's problem and quarter-space model, we compare the FD and FD-FE solutions with that obtained by Carcione (1992). In the FD-FE modeling, we covered a part of the half-space by the finite elements as indicated by dashed lines in Figure 3. Carcione (1992) uses a Zener rheological model and a pseudospectral technique to compute the spatial derivatives. Assuming one relaxation mechanism ($n = 1$ in equations 2 and 27) for each wave type, we can strictly solve the same problem with both algorithms.

The agreement of all three solutions is very good in the case of the homogeneous half-space (HH, the upper part of Fig. 4b). In the case of the welded quarter-spaces (WQ, the lower part of Fig. 4b), we observe a small discrepancy in the amplitude of the reflected Rayleigh wave arriving at about 1.35 sec in the R1 receiver. We performed additional

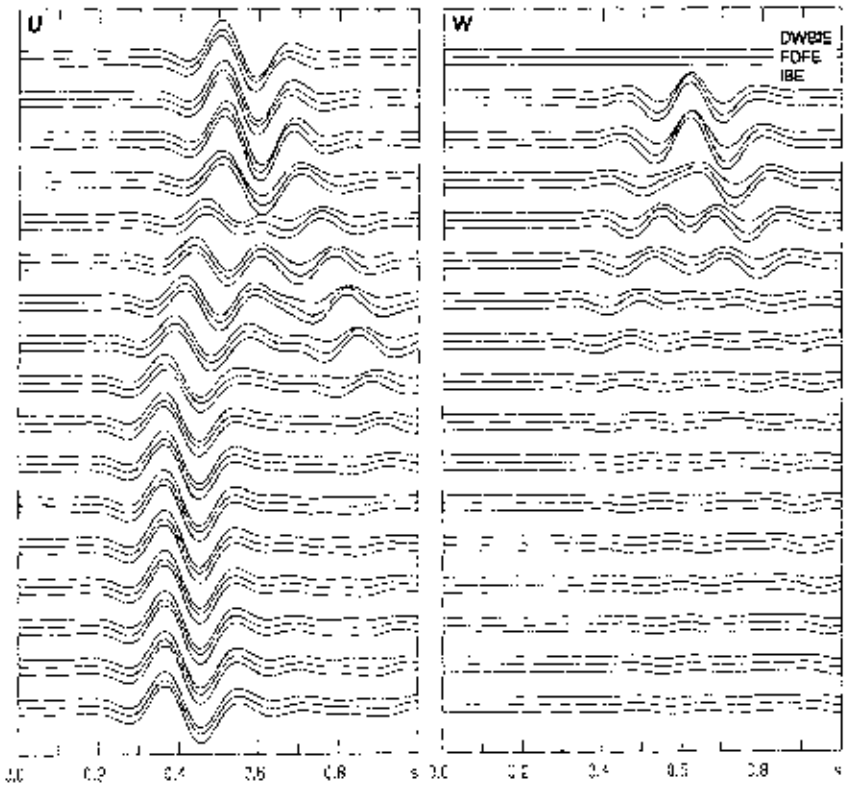

Figure 8. Comparison of the DW-BIE (discrete wavenumber–boundary integral equation) and IBE (indirect boundary element; computed by H. A. Pedersen) solutions with our FD-FE solution for the model of the trapezoidal ridge shown in Figure 7.

computations for the purely elastic medium to find out whether the incorporation of the attenuation or the modeling of the internal discontinuity is responsible for the small discrepancy. Based on the comparison with the finite-difference (PSI) and spectral element (SPEM) methods in Zahradník and Priolo (1995), we suspect that the discrepancy is due to the uncertainty in the vertical interface position (one grid point) present in the pseudospectral method and not due to the incorporation of the attenuation. All three solutions agree very well in the R2 receiver and satisfactorily in the R3 receiver (realizing the small amplitudes in R3 compared with those in R1 and R2).

Inclusion of Topography

We consider two basic types of topographic irregularities: a canyon and a ridge. For the first comparison, we take a model of a semicircular canyon first studied by Trifunac (1971). The model is shown in Figure 5. Since we want to compare in the time domain, we take a solution obtained by Kawase (1988) who used the discrete wavenumber–boundary element method. Kawase demonstrated the accuracy of his method by comparing his solution in the *SH* case with Trifunac's analytical solution.

The canyon is subjected to a plane *P*-wave impinging vertically from below. The time function of the incident wave is given by a Ricker wavelet defined as

$$w_r(\tau) = (2\pi^2 f_c^2 \tau^2 - 1)\exp(-\pi^2 f_c^2 \tau^2),$$

where f_c is the characteristic frequency of the wavelet and $\tau = t\beta/a$ is the nondimensional time (which in the frequency domain corresponds to the nondimensional frequency $f_n = fa/\beta$), a being the radius of curvature of the canyon and β the *S*-wave velocity. Setting $f_c = 1$ and β (m/sec) equal to a (m), we get the wavelength of *S* wave at the characteristic frequency equal to the canyon radius. The *P*-wave velocity is set to be 2β. Based on the grid used in our computation, our solution should be theoretically accurate up to $4f_c$. Both solutions are shown in Figure 6. It is clear that they are in very good agreement. The only slight difference is in the velocity of the Rayleigh waves propagating away from the canyon.

The second topographic geometry that we consider is a ridge of trapezoidal shape (Fig. 7). The base of the ridge is 400 m wide, and its elevation is 150 m. The flanks of the ridge are steeply inclined at 45° from the vertical, while the summital platform is flat and 100 m wide. The *S*-wave and *P*-wave velocities of the medium are 1000 and 2000 m/sec, respectively. The incident seismic wave field is a vertically impinging plane *SV* wave having the time dependence of a Gabor wavelet

$$u_r(t) = \exp\{-[\alpha(t - t_s)/\gamma]^2\}\cos[\omega(t - t_s) + \psi]$$

with $\omega = 2\pi f_p$, $f_p = 5$ Hz, $t_s = 0.36$ sec, $\gamma = 4$, and $\psi = \pi/2$. Receivers are arranged in a linear profile extending from

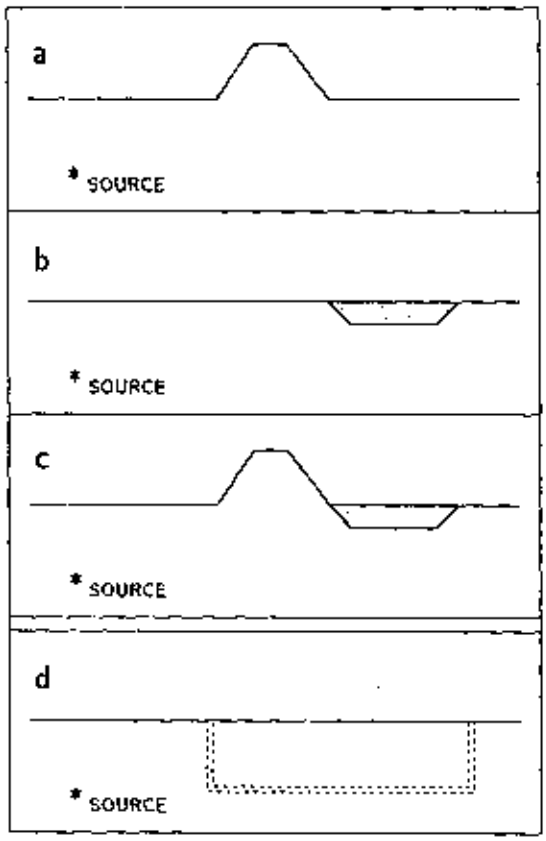

Figure 9. Three models of local structures: (a) trapezoidal ridge, (b) sediment valley, and (c) combined topographic-sedimentary structure. (d) The source radiation and wave propagation in the background medium (i.e., homogeneous half-space) is computed only once. The wave field recorded along the excitation lines (dashed lines) is then used in response computation for each of the structures.

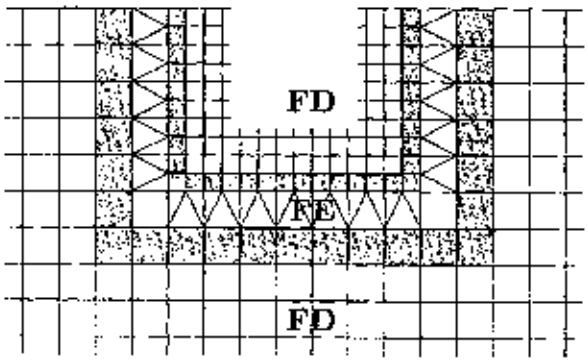

Figure 10. The combined $h \times h$ and $2h \times 2h$ spatial grid. The finite elements are used as a transition zone between the two grids. The shadowed area has the same meaning as that in Figure 2.

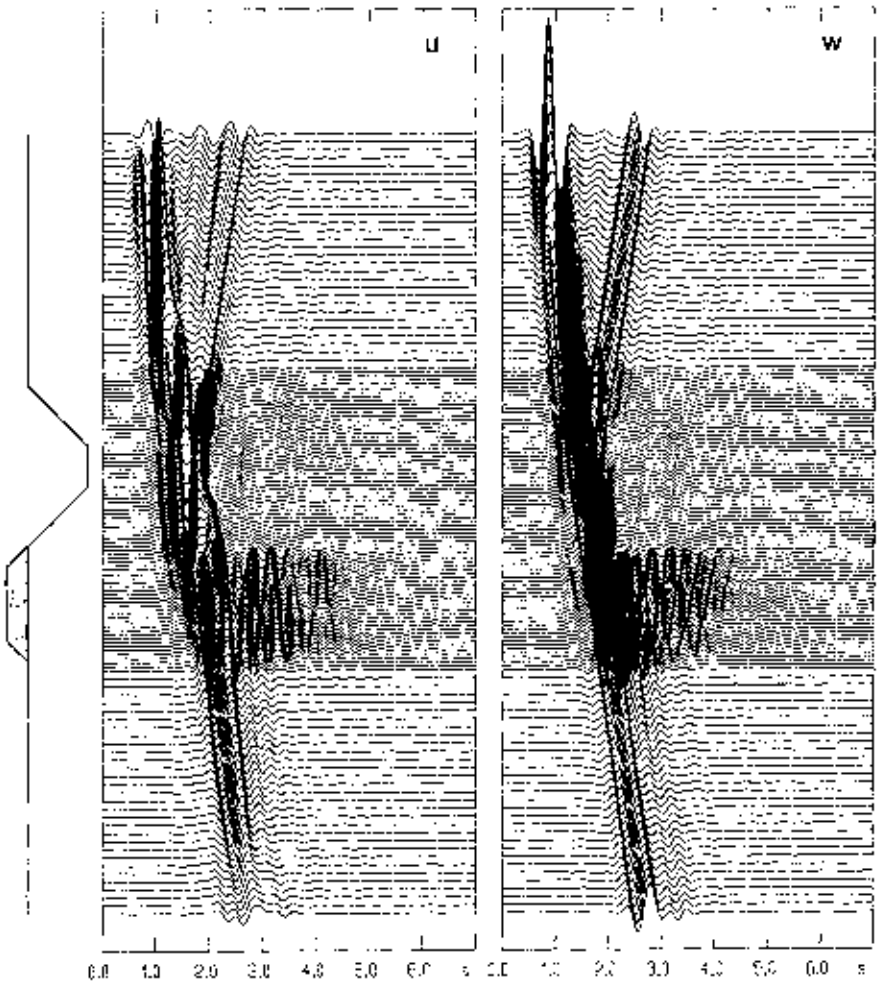

Figure 11. The horizontal (u) and vertical (w) components of the displacements at the receivers along the free surface of the combined topographic-sedimentary structure.

the center of the summital platform to a distance of 200 m from the foot of the ridge. They are equally spaced at 25-m intervals along the horizontal direction. The resulting horizontal and vertical displacement seismograms are presented in Figure 8. We compare our solution with two independent ones: a discrete wavenumber–boundary integral equation method (Gaffet and Bouchon, 1989) and an indirect boundary element method (Pedersen *et al.*, 1994).

The agreement between our solution and the one calculated by the indirect boundary element method is excellent. The results obtained by the discrete wavenumber–boundary integral equation method, although in good general agreement with the other two solutions, slightly underestimate the strength of the diffracted waves. This small discrepancy is attributed to the presence of sharp corners in the topography that are smoothed out in the boundary integral equation formulation.

Based on these numerical tests, we conclude the following: (1) The presented FD scheme and the FD-FE algorithm accurately model anelastic attenuation. (2) The FD-FE algorithm accurately models free-surface topography.

Hybrid Modeling

As shown in Figure 1b, our hybrid modeling consists of two steps. In the first step, the source radiation and wave propagation in the background medium is calculated by the DW method, and the computed wave field U_k is recorded along lines a and b. In the second step, the wave field U_k is applied on lines a and b to excite the wave field in the localized structure and link the total wave field U with the residual wave field U_r.

We have shown in the previous sections that the developed FD scheme and FD-FE algorithm can be used to calculate wave propagation in the U_r and U regions (see Fig. 1b), respectively. Zahradník and Moczo (1996) have demonstrated the validity of the DW-FD coupling algorithm. This is the same method used here for the DW-FD-FE coupling. With respect to the coupling algorithm, the free-surface topography does not mean any change compared to a sedimentary structure with the flat free surface: they both scatter the incident wave field.

In the next numerical example, we want to compute the

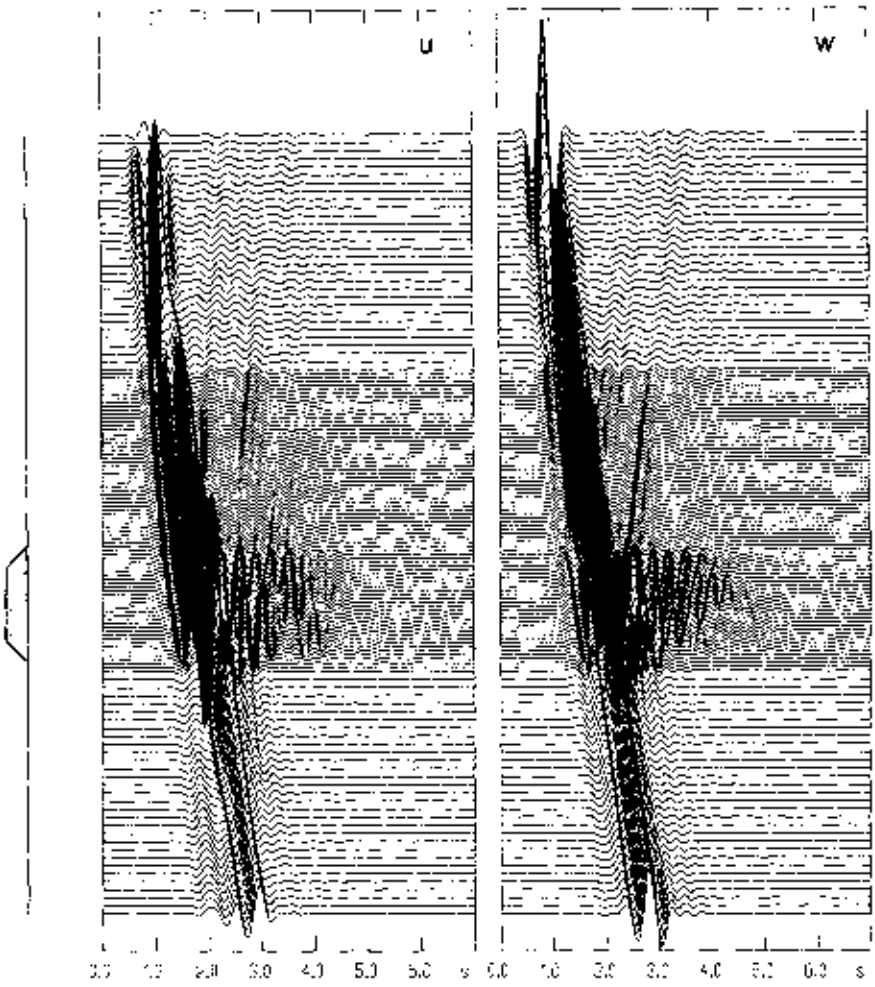

Figure 12. The horizontal (u) and vertical (w) components of the displacements at the receivers along the free surface of the half-space with sediment valley.

response of three localized structures—a ridge, sediment valley, and the ridge neighboring the sediment valley—to the same source radiation (see Figs. 9a through 9c). We can avoid computing the source radiation and background wave propagation three times (i.e., for each of the three structures) by making use of the coupling algorithm. Thus, we first compute the source radiation and background propagation in the absence of both irregularities (i.e., in the homogeneous half-space) and record the wave field along two excitation lines (see Fig. 9d). Second, we apply the recorded wave field on the excitation lines in each of the three computations (one computation for each of the three structures) without including the physical localized source in the computations.

Before we show the numerical results, let us explain one other possible use of the FD-FE combination. In order to make the second-step computation more efficient, we use a $2h \times 2h$ spatial grid for the U_2 region (i.e., outside the excitation rectangle), while we use an $h \times h$ spatial grid inside the excitation rectangle. The link between the $h \times h$ and $2h \times 2h$ grids is accomplished using a strip of finite elements (see Fig. 10). We have checked the performance and accuracy of such a combined grid by comparing it with the regular $h \times h$ grid covering both regions. The use of finite elements between the two FD grids is required because we have not found a stable FD algorithm to link the two grids as in the *SH* case (see Moczo *et al.*, 1996).

In the numerical simulations, we considered the following model and source parameters. The topographic feature is the same trapezoidal ridge as in Figure 7. The sediment valley is 275 and 175 m wide at the surface and at the bottom, respectively. The valley is 55 m deep. The P- and S-wave velocities and the density inside the valley are 900 m/sec, 400 m/sec, and 1500 kg/m^3. The P- and S-wave quality factors are 60 and 40 at a frequency of 6 Hz, and the Futterman $Q(\omega)$ law is assumed. It is approximated using three relaxation mechanisms ($n = 3$) and $\omega_1 = 2\pi 6$ rad/sec. The wave field is due to the downward vertical force acting along the line source that is in 300 m depth and 610 m to the left of the ridge. The time function of the force is given by Gabor wavelet with a dominant frequency $f_p = 2.5$ Hz, $t_s = 0.72$ sec, $\gamma = 4$, and $\psi = \pi/2$. The spatial grid spacing is $h = 5$ m in the U region and 10 m in the U_2 region. The time

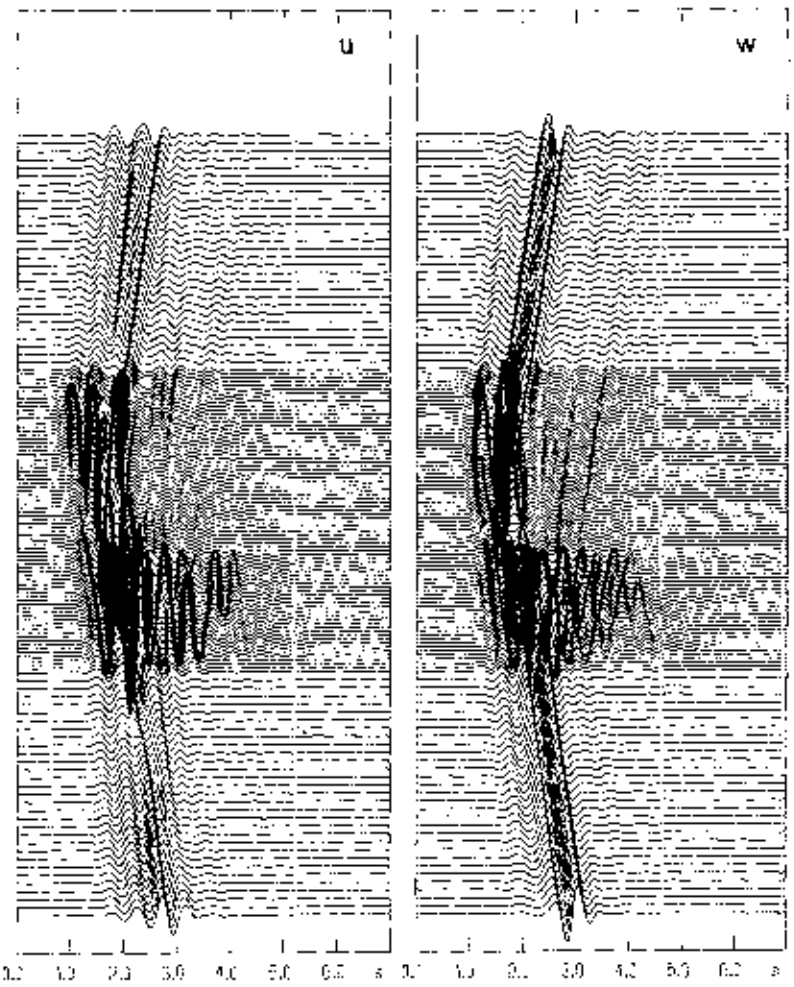

Figure 13. The difference seismograms (seismograms in Fig. 11 minus seismograms in Fig. 12).

step is 0.001 sec. The receivers are equally spaced at 20- and 10-m intervals in the horizontal direction.

Figure 11 shows seismograms at the free surface of the combined topographic-sediment structure. Figure 12 shows seismograms at the free surface of the half-space with sediment valley. Comparison of seismograms in both figures suggests that there are certain differences in the responses of the sediment valleys with and without neighboring ridge. Differences in the waveforms are clearly visible mainly in the horizontal (u) component. Difference seismograms (i.e., seismograms in Fig. 11 minus seismograms in Fig. 12) in Figure 13 exhibit amplitudes and durations that are comparable to those in Figures 11 and 12. Further, we computed the Fourier transfer functions (FTF) by dividing the Fourier spectra of the local responses by the Fourier spectrum of the input signal. In Figure 14, we show the FTF only for the horizontal components since there is practically no difference between the FTF for the vertical components in the valleys with and without neighboring ridge. Both the difference seismograms and FTF confirm that there is a considerable difference in the horizontal components in the responses of the sediment valleys with and without neighboring ridge while the vertical components are very close in both cases (the latter means that the vertical component of the difference seismograms is mainly due to phase shift of very close signals). Thus, we have a strong indication that taking the free-surface topography neighboring the valley can be (depending on the specific structure) important even in the case when we are only interested in the valley response. We do not show the seismograms for purely topographic irregularity and corresponding difference seismograms since in this example the presence of the valley does not change the response of the ridge considerably.

Conclusions

We have developed a new hybrid method to compute the *P-SV* seismic motion at inhomogeneous viscoelastic topographic structures. The method combines the DW (discrete-wavenumber), FD (finite-difference), and FE (finite-

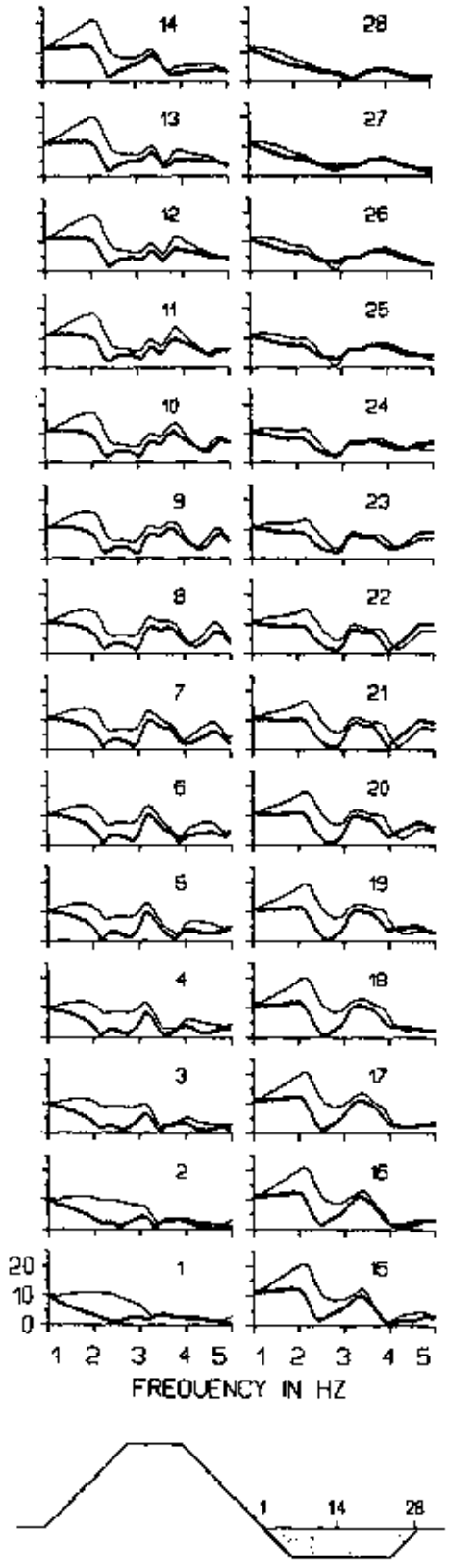

Figure 14. Fourier transfer functions at sites 1 through 28 along the free surface of the sediment valley in the model with neighboring ridge (thick line) and in the model without the ridge (thin line).

element) methods. It represents a generalization of the hybrid DW-FD method suggested recently by Zahradník (1995a) and Zahradník and Moczo (1996) for modeling near-surface structures along with free-surface topography. While the source radiation and wave propagation in the background medium are solved using the DW method, as in the DW-FD method, the inclusion of a free-surface topography is solved by a combined FD FE algorithm.

In developing the FD-FE algorithm for viscoelastic media, we

- applied the explicit heterogeneous elastic FD scheme of Zahradník (1995b) to the viscoelastic medium whose rheology is represented by two generalized Maxwell bodies,
- checked the accuracy of the FD scheme in the viscoelastic medium through numerical comparisons with analytical and independent numerical solutions,
- suggested a way of including the attenuation corresponding to rheology of two generalized Maxwell bodies into the standard FE formulation,
- suggested a time-integration scheme for the FD-FE algorithm,
- have shown that a strip of finite elements can be used as a transition zone between the $h \times h$ and $2h \times 2h$ FD spatial grids in the combined grid, and
- checked the accuracy of the FD-FE algorithm through numerical comparisons with analytical and independent numerical methods for viscoelastic models with a flat free surface and perfectly elastic models with free-surface topography.

Numerical comparisons with independent methods showed that our method is sufficiently accurate.

Using numerical computations, we have shown that accounting for the free-surface topography neighboring a sediment valley can be important even in the case when we are only interested in the valley response. In other words, the ridge can considerably influence the response of the neighboring sediment valley.

Acknowledgments

We thank H. A. Pedersen for providing the IBE solution for a trapezoidal ridge and J. Zahradník for discussion. The reviews by Robert W. Graves and Takao Ohminato helped us to improve the article. This work was supported in part by NATO Linkage Grant ENVIR.LG 940714, Grant Number 2/1064/96, Grant Agency for Science, Slovak Academy of Sciences, Grant Number 205/96/1743, Grant Agency of Czech Republic, and INCO-COPERNICUS Grant PL.963311.

References

Alekseev, A. S. and B. G. Mikhailenko (1980). The solution of dynamic problems of elastic wave propagation in inhomogeneous media by a combination of partial separation of variables and finite difference methods, *J. Geophys.* **48**, 161–172.

Alterman, Z. and D. Loewenthal (1970). Seismic waves in a quarter and three-quarter plane, *Geophys. J. R. Astr. Soc.* **20**, 101–126.

Alterman, Z. and D. Loewenthal (1972). Computer generated seismograms, in *Methods in Computational Physics 12*, B. Alder, S. Fernbach, and M. Rotenberg (Editors), Academic Press, New York, 35–164.

Alterman, Z. and R. Nathaniel (1975). Seismic waves in a wedge, *Bull. Seism. Soc. Am.* **65**, 1697–1719.

Alterman, Z. and A. Rotenberg (1969). Seismic waves in a quarter plane, *Bull. Seism. Soc. Am.* **59**, 347–368.

Bamberger, A., G. Chavent, and P. Lailly (1980). Etude de schemas numeriques pour les equations de l'elastodynamique lineaire: INRIA, No. 032-79, Le Chesnay, France.

Bayliss, A., K. E. Jordan, B. J. LeMesurier, and E. Turkel (1986). A fourth-order accurate finite-difference scheme for the computation of elastic waves, *Bull. Seism. Soc. Am.* **76**, 1115–1132.

Boore, D. M. (1972). Finite difference methods for seismic wave propagation in heterogeneous materials, in *Methods in Computational Physics 11*, B. A. Bolt (Editor), Academic Press, New York, 1–38.

Boore, D., S. C. Harmsen, and S. Harding (1981). Wave scattering from a step change in surface topography, *Bull. Seism. Soc. Am.* **71**, 117–125.

Bouchon, M. (1981). A simple method to calculate Green's functions for elastic layered media, *Bull. Seism. Soc. Am.* **71**, 959–971.

Bouchon, M. and O. Coutant (1994). Calculation of synthetic seismograms in a laterally-varying medium by the boundary element—discrete wavenumber method, *Bull. Seism. Soc. Am.* **84**, 1869–1881.

Bouchon, M., C. A. Schultz, and M. N. Toksöz (1996). Effect of three-dimensional topography on seismic motion, *J. Geophys. Res.* **101**, 5835–5846.

Carcione, J. M. (1992). Modeling anelastic singular surface waves in the Earth, *Geophysics* **57**, 781–792.

Carcione, J. M., D. Kosloff, and R. Kosloff (1988). Wave propagation simulation in a linear viscoelastic medium, *Geophys. J. R. Astr. Soc.* **95**, 597–611.

Emmerich, H. (1989). 2-D wave propagation by a hybrid method, *Geophys. J. Int.* **99**, 307–319.

Emmerich, H. (1992). PSV-wave propagation in a medium with local heterogeneities: a hybrid formulation and its application, *Geophys. J. Int.* **109**, 54–64.

Emmerich, H. and M. Korn (1987). Incorporation of attenuation into time-domain computations of seismic wave fields, *Geophysics* **52**, 1252–1264.

Fäh, D. (1992). A hybrid technique for the estimation of strong ground motion in sedimentary basins, Diss. ETH Nr. 9767, Swiss Federal Institute of Technology, Zurich.

Fäh, D., P. Suhadolc, and G. F. Panza (1993). Variability of seismic ground motion in complex media: the case of a sedimentary basin in the Friuli (Italy) area, *J. Appl. Geophys.* **30**, 131–148.

Frankel, A. and W. Leith (1992). Evaluation of topographic effects on P and S-waves of explosions at the northern Novaya Zemlya test site using 3-D numerical simulations, *Geophys. Res. Lett.* **19**, 1887–1890.

Fuyuki, M. and Y. Matsumoto (1980). Finite difference analysis of Rayleigh wave scattering at a trench, *Bull. Seism. Soc. Am.* **70**, 2051–2069.

Fuyuki, M. and M. Nakano (1984). Finite-difference analysis of Rayleigh wave transmission past an upward step change, *Bull. Seism. Soc. Am.* **74**, 893–911.

Gaffet, S. and M. Bouchon (1989). Effects of two dimensional topographies using the discrete wavenumber-boundary integral equation method in P-SV cases, *J. Acoust. Soc. Am.* **85**, 2277–2283.

Hong, M. and L. J. Bond (1986). Application of the finite difference method in seismic source and wave diffraction simulation, *Geophys. J. R. Astr. Soc.* **87**, 731–752.

Ilan, A. (1977). Finite-difference modeling for P-pulse propagation in elastic media with arbitrary polygonal surface, *J. Geophys.* **43**, 41–58.

Ilan, A. (1978). Stability of finite difference schemes for the problem of elastic wave propagation in a quarter plane, *J. Comp. Phys.* **29**, 389–403.

Ilan, A. and L. J. Bond (1981). Interaction of a compressional impulse with a slot normal to the surface of an elastic half space—II, *Geophys. J. R. Astr. Soc.* **65**, 75–90.

Ilan, A., L. J. Bond, and M. Spivack (1979). Interaction of a compressional impulse with a slot normal to the surface of an elastic half space, *Geophys. J. R. Astr. Soc.* **57**, 463–477.

Ilan, A. and D. Loewenthal (1976). Instability of finite difference schemes due to boundary conditions in elastic media, *Geophys. Prosp.* **24**, 431–453.

Ilan, A., A. A. Ungar, and Z. Alterman (1975). An improved representation of boundary conditions in finite difference schemes for seismological problems, *Geophys. J. R. Astr. Soc.* **43**, 727–745.

Jih, R.-S., K. L. McLaughlin, and Z. A. Der (1988). Free-boundary conditions of arbitrary polygonal topography in a two-dimensional explicit elastic finite-difference scheme, *Geophysics* **53**, 1045–1055.

Kawase, H. (1988). Time-domain response of a semi-circular canyon for incident SV, P, and Rayleigh waves calculated by the discrete wavenumber boundary element method, *Bull. Seism. Soc. Am.* **78**, 1415–1437.

Kummer, B., A. Behle, and F. Dorau (1987). Hybrid modeling of elastic-wave propagation in two-dimensional laterally inhomogeneous media, *Geophysics* **52**, 765–771.

Levander, A. (1988). Fourth-order finite-difference P-SV seismograms, *Geophysics* **53**, 1425–1436.

Luo, Y. and G. Schuster (1990). Parsimonious staggered grid finite-differencing of the wave equation, *Geophys. Res. Lett.* **17**, 155–158.

Madariaga, R. (1976). Dynamics of an expanding circular fault, *Bull. Seism. Soc. Am.* **67**, 163–182.

McLaughlin, K. L. and R.-S. Jih (1988). Scattering from near-source topography: teleseismic observations and numerical simulations, *Bull. Seism. Soc. Am.* **78**, 1399–1414.

Mikhailenko, B. G. and V. I. Korneev (1984). Calculation of synthetic seismograms for complex subsurface geometries by a combination of finite integral Fourier transform and finite-difference techniques, *J. Geophys.* **54**, 195–206.

Moczo, P. and P.-Y. Bard (1993). Wave diffraction, amplification and differential motion near strong lateral discontinuities, *Bull. Seism. Soc. Am.* **83**, 85–106.

Moczo, P. and F. Hron (1992). The sensitivity study of seismic response of sediment-filled valleys with respect to quality factor distributions, in *Proc. of the International Symposium on the Effects of Surface Geology on Seismic Motion*, 25–27 March 1992, Odawara, Japan, Vol. 1, 263–268.

Moczo, P., F. Hron, J. Kristek, and F. Hron (1996). Amplification and differential motion due to an antiplane 2D resonance in the sediment valleys embedded in a layer over the half space, *Bull. Seism. Soc. Am.* **86**, 1434–1446.

Moczo, P., A. Rovelli, P. Labák, and L. Malagnini (1995). Seismic response of the geologic structure underlying Roman Colosseum and a 2-D resonance of a sediment valley, *Ann. Geofis.* **38**, 939–956.

Muir, F., J. Dellinger, J. Etgen, and D. Nichols (1992). Modeling elastic fields across irregular boundaries, *Geophysics* **57**, 1189–1193.

Munasinghe, M. and G. W. Farnell (1973). Finite-difference analysis of Rayleigh wave scattering at vertical discontinuities, *J. Geophys. Res.* **78**, 2454–2466.

Ohminato, T. and B. A. Chouet (1997). A free surface boundary condition for including 3D topography in the finite-difference method, *Bull. Seism. Soc. Am.* **87**, 494–515.

Ohtsuki, A. and K. Harumi (1983). Effect of topography and subsurface inhomogeneities on seismic SV waves, *Earthquake Eng. Struct. Dyn.* **11**, 441–462.

Ohtsuki, A., H. Yamahara, and K. Harumi (1984). Effect of topography and subsurface inhomogeneity on seismic Rayleigh waves, *Earthquake Eng. Struct. Dyn.* **12**, 37–58.

Pedersen, H. A., F. J. Sánchez-Sesma, and M. Campillo (1994). Three-dimensional scattering by two-dimensional topographies, *Bull. Seism. Soc. Am.* **84**, 1169–1183.

Ravelli, A., A. Caserta, L. Malagnini, and F. Marra (1994). Assessment of potential strong ground motions in the city of Rome, *Ann. Geofis.* **37**, 1745–1769.

Sawada, Y. (1992). Geotechnical data, in *Proc. of the International Symposium on the Effects of Surface Geology on Seismic Motion*, 25–27 March 1992, Odawara, Japan, Vol. II, 29–42.

Serón, F. J. and J. I. Badal (1992). Computational seismic modelling based on finite elements, *Rev. Geofis.* **48**, 37–45.

Serón, F. J., F. J. Sanz, and M. Kindelán (1989). Elastic wave propagation with the finite element method, IBM, European center for scientific and engineering computing, ECE-0028.

Serón, F. J., F. J. Sanz, M. Kindelán, and J. I. Badal (1990). Finite-element method for elastic wave propagation, *Appl. Num. Meth.* **6**, 359–368.

Smith, W. D. (1975). The application of finite element analysis to body wave propagation problems, *Geophys. J. R. Astr. Soc.* **42**, 747–768.

Trifunac, M. D. (1971). Surface motion of a semi-cylindrical alluvial valley for incident plane SH waves, *Bull. Seism. Soc. Am.* **61**, 1755–1770.

Van den Berg, A. (1984). A hybrid solution for wave propagation problems in regular media with bounded irregular inclusions, *Geophys. J. R. Astr. Soc.* **79**, 3–10.

Virieux, J. (1986). P-SV wave propagation in heterogeneous media: velocity-stress finite-difference method, *Geophysics* **51**, 889–901.

Yuan, Y., B. Yong, and S. Huang (1992). Damage distribution and estimation of ground motion in Shidian (China) basin, in *Proc. of the International Symposium on the Effects of Surface Geology on Seismic Motion*, 25–27 March 1992, Odawara, Japan, Vol. I, 281–286.

Zahradník, J. (1995a). Comment on "A hybrid method for the estimation of ground motion in sedimentary basins: Quantitative modeling for Mexico City" by D. Fah, P. Suhadolc, St. Mueller, and G. F. Panza, *Bull. Seism. Soc. Am.* **85**, 1268–1270.

Zahradník, J. (1995b). Simple elastic finite difference scheme, *Bull. Seism. Soc. Am.* **85**, 1879–1887.

Zahradník, J., J. Jech, and P. Moczo (1990). Absorption correction for computations of a seismic ground response, *Bull. Seism. Soc. Am.* **80**, 1382–1387.

Zahradník, J. and P. Moczo (1996). Hybrid seismic modeling based on discrete-wavenumber and finite-difference methods, *Pure Appl. Geophys.* **148**, 21–38.

Zahradník, J., P. Moczo, and F. Hron (1993). Testing four elastic finite-difference schemes for behaviour at discontinuities, *Bull. Seism. Soc. Am.* **83**, 107–129.

Zahradník, J., P. Moczo, and F. Hron (1994). Blind prediction of the site effects at Ashigara Valley, Japan, and its comparison with reality, *Natural Hazards* **10**, 149–170.

Zahradník, J. and E. Priolo (1995). Heterogeneous formulations of elastodynamic equations and finite-difference schemes, *Geophys. J. Int.* **120**, 663–676.

Zienkiewicz, O. C. and R. L. Taylor (1989). *The Finite Element Method*, 4th ed., Vol. 2, McGraw-Hill Book Co., New York.

Geophysical Institute
Slovak Academy of Sciences
Dúbravská cesta
842 28 Bratislava, Slovak Republic
(P. M., E. B., J. K.)

Osservatorio Geofisico Sperimentale
P.O. Box 2011
34016 Trieste, Italy
(J. M. C.)

Laboratoire de Géophysique Interne et Tectonophysique
Université Joseph Fourier
BP53X
38041 Grenoble Cedex, France
(M. B.)

Manuscript received 6 January 1996.